

FINAL YEAR PROJECT REPORT

NAME:	William Davie
DEGREE COURSE:	Physics (BSc)
PROJECT TITLE:	Structural Behavior of Two-Dimensional Skyrmions under Circular Confinement
YEAR OF SUBMISSION:	2023
SUPERVISOR:	Dr Thomas Machon
NUMBER OF WORDS:	5500



Declaration

This project is a result of independent work, including code development, collection of results and creation of diagrams. My partner, Daniel Gillam, and I discussed and compared results to verify our own findings. During meetings my supervisor taught key concepts, necessary for developing a strong understanding of the topics discussed. I had access to BluePebble throughout the project.

Acknowledgements

I'd like to thank all those within the School of Physics who have consistently provided teaching of the highest calibre. Notably, my supervisors Dr Simon Hanna (Summer 2023) and Dr Thomas Machon (Spring 2024) for guidance throughout the research process, allowing me to produce valuable work and develop as a scientist. Thank you to my friends and family for your love and support.

Preface

Alongside the results obtained, this report attempts to demonstrate a broad depth of understanding. Therefore, I have included; i) fundamental theory and background, ii) personally-made diagrams wherever possible, iii) extended derivations, iv) supplementary material including code and videos. In some cases, these features may not be necessary, though, I hope they help the reader find value and clarity in both my understanding and the presented work.

Abstract

Two-dimensional skyrmions are simulated under circular confinement, where the orientation of the director $\mathbf{n}(x, y)$ is constrained at the boundary ($\mathbf{n}(\mathbf{R}) = \mathbf{e}_z$). Since the director has a preference to twist on a length scale p (ground state helical pitch), these boundary conditions introduce frustration [1]. When local frustration is induced, the Helfrich-Hurault instability is observed [2]; the skyrmion undulates and exhibits a complex superposition of length scales $\approx np$. When global frustration is induced, the introduction of a 2π twist (wavelength of twist = λ_t) is observed. By simulating a number of $n\pi$ twisted skyrmions, the collapse ($p >> \lambda_t$) and stabilisation ($p \approx \lambda_t$) of twist is shown.

Contents

1	Introduction	1
1.1	Motivation	1
1.2	Defining Skyrmions	1
1.2.1	Topology	1
1.2.2	Configuration Diversity	2
1.3	Skyrmions in Magnetic Materials	2
1.3.1	Landau Theory	3
1.3.2	Exchange Interaction	4
1.3.3	Dzyaloshinskii-Moriya Interaction	5
1.4	Skyrmions in Liquid Crystals	5
1.4.1	Frank free energy	6
1.5	Energetic Stability	7
1.5.1	Frustration and the Helfrich-Hurault instability	7
1.6	Project Aims and Scope	8
2	Methodology	9
2.1	Simulation	9
2.1.1	Limitations	10
2.1.2	Additional Information	11
3	Results and Discussion	12
3.1	Pilot Simulation	12
3.2	Varied grid size	16
3.3	$n\pi$ Twisted Skyrmions	19
4	Conclusion	21
4.1	Further Work	21
5	Appendix	25
5.1	A: Derivations	25
5.1.1	A.1 Spin Hamiltonian in the Continuum Limit	25
5.1.2	A.2 One-constant approximation	25
5.1.3	A.3 Derivative of Energy Functional	26
5.1.4	A.4 Expected energy relationship	27
5.2	B: Tables	28
5.3	C: Supplementary Material	29

1 Introduction

1.1 Motivation

Topologically stable, chiral spin structures, known as skyrmions, have been observed in thin-layers of ferromagnets [3, 4] and liquid crystals [5]. Since their observation, skyrmions have driven a broad movement of research due to their structural complexity and potential as spintronic storage devices [6]. Their smooth twisted structure mediates a stability not observed in other solitonic structures, enabling the transfer of information under the influence of an external current [7]. Characterized by a topological charge Q [8], skyrmions are considered topologically protected and therefore, are prevented from continuous transformations to a saturated, uniform state. To this day, a variety of complex skyrmions have been theoretically predicted [8] and observed [9], demonstrating the high density of information stable skyrmions can possess. Prior research has shown the stability of complex skyrmion structures is often realized by some form of external control, such as geometric confinement [10] or the introduction of an outer skyrmion bag [11]. Here, computational methods are used to explore the stability of skyrmions under a specific set of circular boundary conditions, focusing on the structural influence of chirality, imposed by the Frank free energy term $(q_0 + \mathbf{n} \cdot \nabla \times \mathbf{n})^2$ [10]. Where $2\pi/q_0$ is the helical pitch of the ground state.

We provide insight into the exhibited stabilisation mechanisms when a skyrmion is subject to frustration, demonstrating how chiral condensed matter systems interact with their surrounding environment. Studies of this kind may have significance in understanding how stability can be enhanced, or instability suppressed.

1.2 Defining Skyrmions

1.2.1 Topology

Skyrmions are fundamentally defined by their topology [12]. Topology refers to the classification of geometric objects with invariant properties under continuous deformations. All objects are defined within a space, where spaces may be n-dimensional vector spaces, such as a 2D plane \mathbb{R}^2 or curved spaces, like the surface of a sphere S^2 (note S^2 is a 2D space that cannot be embedded in \mathbb{R}^2). Within any space it is possible to define paths that represent geometric objects; paths that can be continuously transformed into one another are within the same topological group [13].

Skyrmions correspond to the stereo-graphic projection¹ of a geometric path defined on a sphere S^2 onto a disk D^2 (Fig. 1). In particular, one which consists of a field variable $\mathbf{n} = (n_x, n_y, n_z)$ that wraps around S^2 an integer number of times. This ‘winding number’ is a fundamental topological property conserved under continuous deformations [12]. Consequently, skyrmions inherit a topological charge Q ;

$$Q = \frac{1}{4\pi} \int_D \mathbf{n} \cdot \left(\frac{\partial \mathbf{n}}{\partial x} \times \frac{\partial \mathbf{n}}{\partial y} \right) dx dy \quad (1.1)$$

¹A method used to map a sphere onto a plane, the south-pole is projected onto the origin and the rest of the sphere is projected via lines tangential to its surface [14].

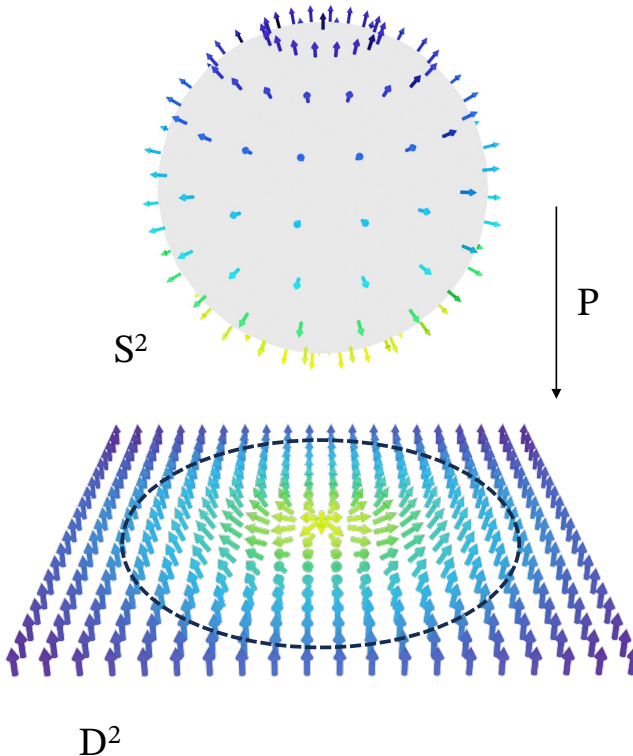


Figure 1: Stereo-graphic projection (\mathbf{P}) of a winding director field $\mathbf{n} = (n_x, n_y, n_z)$ from a sphere S^2 onto a disk D^2 . The resulting field defined over D^2 is a 2D skyrmion with topological charge $Q = 1$.

quantifying the number of times $\mathbf{n}(x, y)$ wraps around S^2 [15]. An important property of skyrmions is that changing Q is greatly unfavourable and in mathematically idealised cases would require infinite energy [16]. Therefore, skyrmions with $Q \in \mathbb{Z}$ are considered topologically stable. Note, the condition $\mathbf{n} \cdot \mathbf{n} = 1$ (unit-magnitude director) is required for eq.(1.1) to return an integer value.

1.2.2 Configuration Diversity

A rich diversity of skyrmion configurations are able to satisfy $Q \in \mathbb{Z}$. For example, $n\pi$ twisted skyrmions (Fig. 2b) alternate in topological charge between $Q = 0$ (even n) and $|Q| = 1$ (odd n) [17], it was initially assumed these twisted skyrmions were the only possible stable skyrmion states [18]. However, recently it has been shown clusters of skyrmions with an arbitrary large topological charge $Q = N$ are able to remain stable [8]. This diversity and topological complexity of unique skyrmion states motivates a large portion of research within the field, by studying numerous skyrmion states a broader picture of topological and structural behaviour is obtained.

1.3 Skyrmions in Magnetic Materials

It is now useful to provide context of how skyrmions exist in nature, importantly, the contributions to an energy functional.

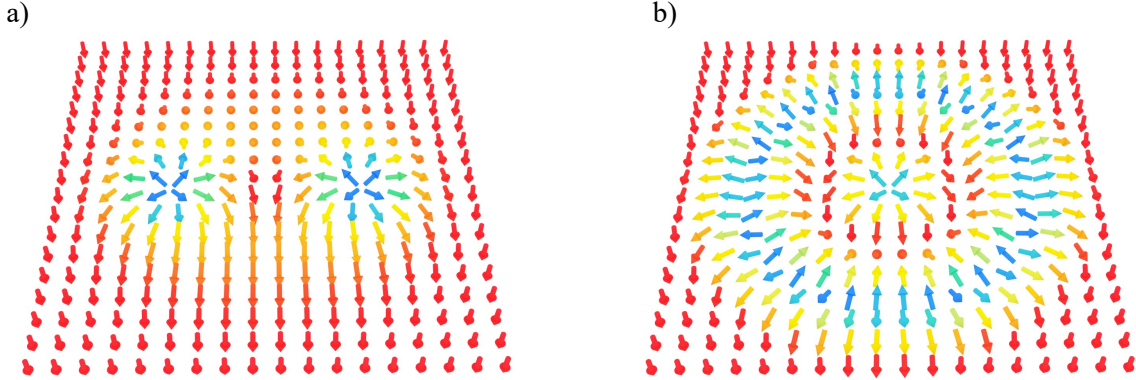


Figure 2: a) $|Q| = 2$ skyrmion b) 3π twisted skyrmion

1.3.1 Landau Theory



Figure 3: a) A 1D array of disordered magnetic moments. b) A fully ordered 1D array of magnetic moments, representing a saturated ferromagnet.

Consider a one dimensional array of randomly ordered magnetic moments (Fig. 3a). At some critical temperature T_c , this material will undergo a magnetic phase transition, that is, magnetic moments will transition from a state of dis-order to a state of order [19] (Fig. 3b). A theory of magnetic moment ordering was developed by Lev Landau [14, 20], it predicts magnet materials reach equilibrium via the minimisation of a free energy functional:

$$F(T, M) - F_0 = a_0(T - T_c)M^2 + bM^4 \quad (1.2)$$

Where a_0 and b are constants, T is temperature and M is magnetisation, which corresponds directly to the ordering of magnetic moments \mathbf{m} [21]:

$$M = \frac{1}{V} \sum_i \mathbf{m}_i \quad (1.3)$$

When $T > T_c$, $F(T, M)$ has a single minima at the origin, representing a fully dis-ordered state (at the limit of infinity random moments cancel to 0). When $T < T_c$, $F(T, M)$ has two minima (Fig. 4a) and in most cases, the entire material will fall into one of either minima, leaving a fully ordered state (a saturated ferromagnet, Fig. 3b). However, it is possible for half of the material to fall into the negative mimina and half to fall into the positive minima. In such case, the array of magnetic moments twist between a positive ($+M_0$) and negative ($-M_0$) magnetisation (Fig. 4c), this is known as a kink [12, 14].

A kink is a remarkably stable structure, as to remove it, all magnetic moments at one minima must

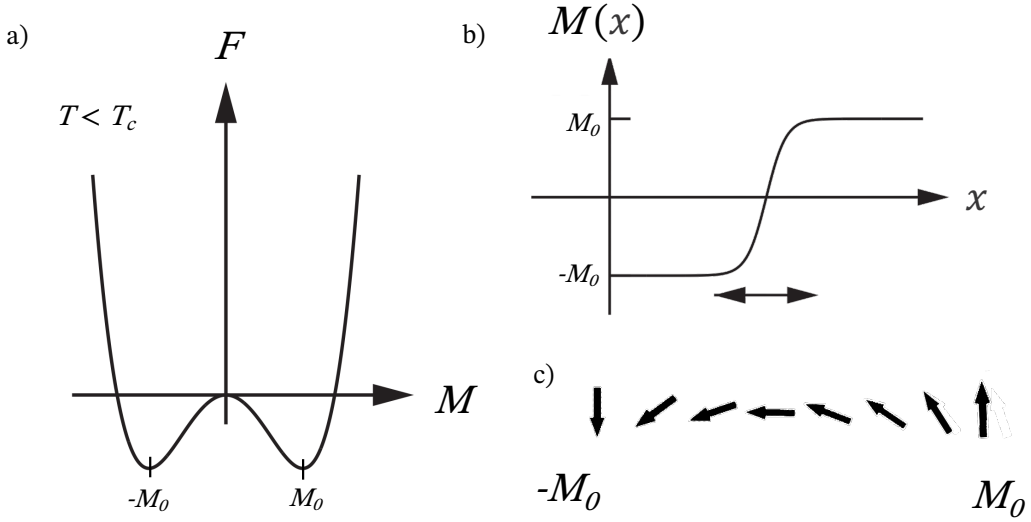


Figure 4: a) A plot of Landau free energy eq.(1.2) where temperature T is below the critical temperature T_c and M is magnetization (ordering parameter). When a magnetic material is split between the negative and positive minima, a magnetic kink forms. b, c) A magnetic kink, magnetic moments smoothly transition from $+M_0$ to $-M_0$. The resulting twisted structure is stabilised by the DMI interaction, see 1.3.3. (a) and (b) are taken from [14].

be transferred over a hump of potential to reach the other minima. This ‘energetic constraint’ (i.e. Fig. 4a) ensures twisted magnetic structures employ a protected winding number, leading to director fields with integer topological charge, eq.(1.1). In fact, by extending this theory of ordering to three dimensions, a spherical mono-pole forms² [14], where its stereo-graphic projection agrees exactly the topological definition of skyrmions.

Note, additional dimensions do add complexity to the system. Un-like a kink, there are many ‘winding moment configurations’ that smoothly transition from $+M_0$ to $-M_0$, as seen for skyrmions in the previous section.

1.3.2 Exchange Interaction

The short description of Landau’s theory demonstrates why twisted magnetic structures (including skyrmions) are able to form and remain stable, however, to understand the fundamental interactions that underpin eq.(1.2), it is helpful to turn to quantum mechanics.

Within any material, electrons occupy space (orbitals) around a corresponding atomic core³[22]. Where each electron carries an ‘intrinsic angular momentum’ known as its spin [23]. Spin \mathbf{S} is a fundamental quantum (quantized) property, that follows the fundamental Pauli exclusion principle. The principle states electrons of opposing (anti-parallel) spin are ‘allowed’ to occupy the same region

²A mono-pole is entirely analogous to a kink, magnetic moments on a sphere twist from $+M_0$ on the north pole to $-M_0$ on the south pole. The sphere in Fig. 1 is a mono-pole.

³Note the simplification, orbitals represent a probabilistic distribution of where an electron may be at any instant.

of space and electrons of parallel spin are not. This therefore governs interactions between electrons on neighbouring atomic sites. Notably, in ferromagnetic materials it is energetically favourable for electron spin to align parallel (when $T < T_c$), spreading out and reducing Coulomb potential energy. This phenomena is known as the exchange interaction and can be represented mathematically by the Heisenberg Hamiltonian [24]:

$$H_{\text{Ex}} = J \sum_{i,j} \mathbf{S}_i \cdot \mathbf{S}_j \quad (1.4)$$

The magnetic moment at each atomic site can be interpreted as the combined spin of local electrons. Therefore, \mathbf{S}_i represents the i^{th} magnetic moment and J is a coupling co-efficient⁴.

1.3.3 Dzyaloshinskii-Moriya Interaction

As shown (Fig. 4), Landau's theory eq.(1.2) predicts the possibility of a twisted arrangement of magnet moments in equilibrium. Such ordering cannot be the case if the entire system is governed by eq.(1.4). Therefore, an additional fundamental interaction must exist to stabilise twisted structures (such as skyrmions), known as the Dzyaloshinskii-Moriya Interaction [25]:

$$H_{\text{DM}} = \sum_{i,j} \mathbf{D}_{i,j} \cdot (\mathbf{S}_i \times \mathbf{S}_j) \quad (1.5)$$

Where $D_{i,j}$ determines the strength of the interaction, it is included in the sum due to a dependence on moment orientation. Hence the Hamiltonian for the entire system⁵ can be written:

$$H = J \sum_{i,j} \mathbf{S}_i \cdot \mathbf{S}_j + \sum_{i,j} \mathbf{D}_{i,j} \cdot (\mathbf{S}_i \times \mathbf{S}_j) \quad (1.6)$$

A system governed by this Hamiltonian eq.(1.6) exhibits a helical spin state (Fig. 5b). Under the continuum limit over a 2D plane, an energy functional dependant on the director \mathbf{n} is obtained [26] (Appendix A.1, 5.1.1);

$$E = \int \frac{J}{2} |\nabla \mathbf{n}|^2 + D(\mathbf{n} \cdot \nabla \times \mathbf{n}) dx dy \quad (1.7)$$

eq.(1.7) plays an important role within this project. Given a unit-magnitude director $\mathbf{n}(x,y)$ satisfying the topological conditions of a skyrmion, the minimisation of eq.(1.7) will entirely govern the numerical evolution of the simulated systems.

1.4 Skyrmions in Liquid Crystals

Solitonic twisted structures, including skyrmions, also exist in liquid crystals. In particular, they are observed in thin layers of chiral nematic (cholesteric) liquid crystals [27]. Liquid Crystals are a phase of matter that exhibit thermodynamic properties of both liquids (eg. flow) and ordered solids [28]. Calamitic liquid crystals consist of rod-like molecules, where long axis orientation may be represented by a director field $\mathbf{n}(\mathbf{r})$. The simplest calamitic phase, with long range orientational

⁴The sign of J will determine whether a material exhibits ferromagnetic or antiferromagnetic ordering.

⁵For simplicity and project relevance, anisotropy and external fields are ignored.

symmetry, analogous to a ferromagnetic, is the nematic phase (Fig. 5a). For twisted structures, such as skyrmions, to remain stable in nematic liquid crystals, molecules must be made chiral⁶. Chirality has a profound affect on the liquid crystal's properties, notably, enabling the formation and stability of helical structures with helical pitch p (Fig. 5b). This phase, with helical order, is uniquely classified as the chiral nematic (cholesteric) phase [30].

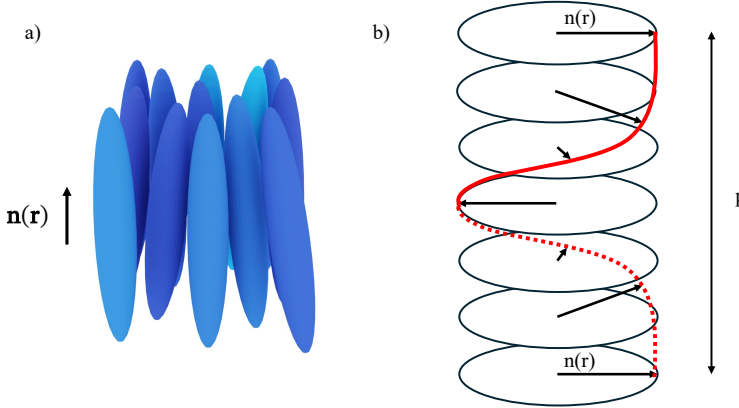


Figure 5: a) Neumatic phase, rod-like molecules are aligned parallel with long range orientational symmetry. b) Helical superstructure, in the cholesteric phase, stable helical structures form. The director $n(r)$ twists 360° over a distance p , the helical pitch. A mathematical description of the helix is given by eq.(1.12).

Note Fig. 5b also resembles a helical magnetic spin structure and is similar in nature to the magnetic kink (Fig. 4c). This is no coincidence, Landau theory is in fact a general description of phase transitions that can be applied to both magnetic materials and liquid crystals [31].

1.4.1 Frank free energy

Distortions in the nematic director $n(r)$, such as skyrmions and structures alike, come with an 'energetic cost' on the Helmholtz free energy:

$$F = F_0 + F_d$$

We consider the one-constant approximation for the distortion energy (Frank free energy) F_d [11, 32];

$$F_d = \frac{K}{2} [(\nabla \cdot n)^2 + (q_0 + n \cdot \nabla \times n)^2 + ((n \cdot \nabla)n)^2] \quad (1.8)$$

where K is an elastic constant and $q_0 = 2\pi/p$, where p is the helical pitch (Fig. 5b). Note the term;

$$F_{ch} = \frac{K}{2} (q_0 + n \cdot \nabla \times n)^2 \quad (1.9)$$

is imposed by chirality, analogous to the DMI (eq.(1.5)), this term stabilises twisted structures. Eq.(1.8) may be simplified and represented as an energy functional (Appendix A.2, 5.1.2):

⁶'I call any geometrical figure or group of points "chiral", and say it has chirality, if its image in a plane mirror, ideally realized, cannot be brought to coincide with itself' - Lord Kelvin [29]

$$E(\mathbf{n}) = \int \frac{K}{2} |\nabla \mathbf{n}|^2 + B(\mathbf{n} \cdot \nabla \times \mathbf{n}) dx dy \quad (1.10)$$

Importantly, we find eq.(1.10) and eq.(1.7) are mathematically equivalent. Therefore, our simulations represent a ‘general’ system. However, throughout this report we use the labels K and B .

1.5 Energetic Stability

This project considers the evolution of a 2D skyrmion as it approaches energetic stability. Specifically, we consider a case where the orientation of the director $\mathbf{n}(x, y)$ is constrained perpendicular to the plane on which it is defined, at any point outside a circle with radius R . The evolution is performed via the minimisation of the generalised energy functional obtained in previous sections eq.(1.7, 1.10), stability is reached when the following condition is satisfied (Appendix A.3, 5.1.3):

$$\frac{\delta E}{\delta \mathbf{n}} = 2B(\nabla \times \mathbf{n}) - K\nabla^2 \mathbf{n} = 0 \quad (1.11)$$

The presence of $\nabla \times \mathbf{n}$ suggests the skyrmion (embedded in $\mathbf{n}(x, y)$) may twist in search of stability, this is in fact widely observed [10, 11, 33]. In such case, the employment of boundary conditions that enforce constant orientation will introduce frustration⁷ [1] and consequently cause unique structural behaviour.

1.5.1 Frustration and the Helfrich-Hurault instability

A common mechanism to relieve geometric frustration, particularly in the context of liquid crystals, is the Helfrich-Hurault (HH) instability [2]. The phenomena is relevant in systems where it is energetically favourable to introduce defects, namely, by introducing undulations. The undulations attempt to maintain a length scale which may be prevented by boundary conditions (Fig. 6). The preferred length scale corresponding to our system is found analytically by considering the ground state solution to the Frank free energy eq.(1.10):

$$\mathbf{n}_g = (\cos(q_0 z), \sin(q_0 z), 0) \quad (1.12)$$

This state corresponds to the helical structure previously mentioned as a consequence of chirality and the DMI interaction. All its rotated variants satisfy the condition $\mathbf{n} \cdot \nabla \times \mathbf{n} = -q_0$ and thus define the preferred length scale $2\pi/q_0$. At longer length-scales, repetition of the helix can be regarded as ‘pseudo-layers of constant orientation’ with spacing $2\pi/q_0$ [2].

Since the ground state eq.(1.12) is energetically preferred, an expected energy against B eq.(1.10) relationship ($B = Kq_0$) can be defined;

$$E = - \int \frac{B^2}{2} dA \quad (1.13)$$

derived in Appendix A.4; 5.1.4.

⁷‘Frustration’ in this context refers to the mathematical conflict between the directors tenancy to twist and the enforced boundary conditions.

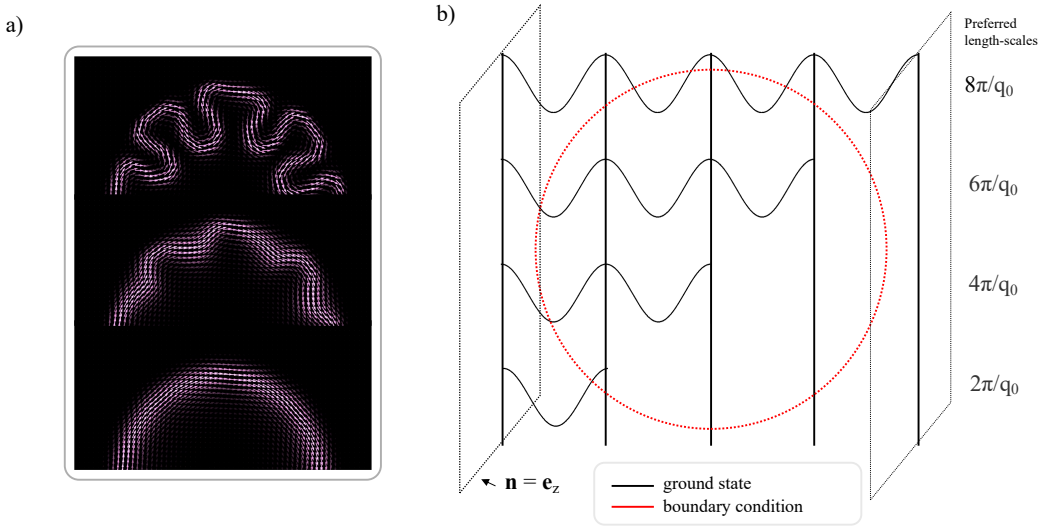


Figure 6: **a)** Formation of Helfrich-Hurault undulations on a circular boundary. **b)** Diagram to demonstrate the mis-alignment between enforced boundary conditions and the helical ground state.

1.6 Project Aims and Scope

Within this section, we have given a short overview of fundamental ideas and mathematics that lead to the energy functional underpinning our simulation. The stable topology of skyrmions in conjunction with frustration induced by boundary conditions opens a door for in-depth analysis. We aim to develop an understanding of frustration release mechanisms and therefore, the structural behaviour of skyrmions under such conditions. It is my hope that the results provided align, to some extent, with the motivations given: Building on prior research of skyrmion stability in confined spaces and leaving an opening for additional investigation.

We run simulations within an ‘effective system’ corresponding to a real space system projected onto a grid. Studying the effect of two key variables i) B values, ensuring a change in the preferred length scale p (or helical pitch) ii) Initial conditions including grid size and skyrmion twist. The results have been presented visually and are open for additional interpretation beyond the scope of this work. Furthermore a github repo includes code and supplementary videos (Appendix C, 5.3).

2 Methodology

2.1 Simulation

Our simulation aims to find numerical solutions to the stability condition:

$$\frac{\delta E}{\delta \mathbf{n}} = 2B(\nabla \times \mathbf{n}) - k\nabla^2 \mathbf{n} = 0 \quad (2.1)$$

We have set up in the following way: An initial director $\mathbf{n}(x, y)$ is defined over a 2D grid, demonstrated by Fig. 7a. For simplification, we only consider the case $a = a_x = a_y = 1$, $N_x = N_y = N$. To correctly initialize a director \mathbf{n} on each grid point (x, y) that satisfies the topological definition of a skyrmion, complex analysis is used:

$$n_x = \frac{2\text{Re}(\psi)}{1 + |\psi|} \quad n_y = \frac{2\text{Im}(\psi)}{1 + |\psi|} \quad n_z = \frac{|\psi| - 1}{1 + |\psi|}$$

Where ψ is a function of the complex number $x + iy$. For example, to initialize a $Q = +1$ skyrmion with radius R , ψ is defined as:

$$\psi = \frac{(|x + iy|^2 - R^2)\alpha e^{i\theta}}{x - iy} \quad (2.2)$$

Where the complex number $\alpha e^{i\theta}$ is a constant scaling parameter. This equation ensures $\mathbf{n} \cdot \mathbf{n} = 1$, $\mathbf{n}(x, y) = -\mathbf{e}_z$ when $x^2 + y^2 > R^2$ and $\mathbf{n}(0, 0) = \mathbf{e}_z$, the supplementary code includes a number of additional ψ formula with corresponding states $\mathbf{n}(x, y)$.

Once $\mathbf{n}(x, y)$ is defined, gradient descent is applied to find a local minimum of the functional $E(\mathbf{n})$. Iterative steps are taken in the opposite direction to the gradient:

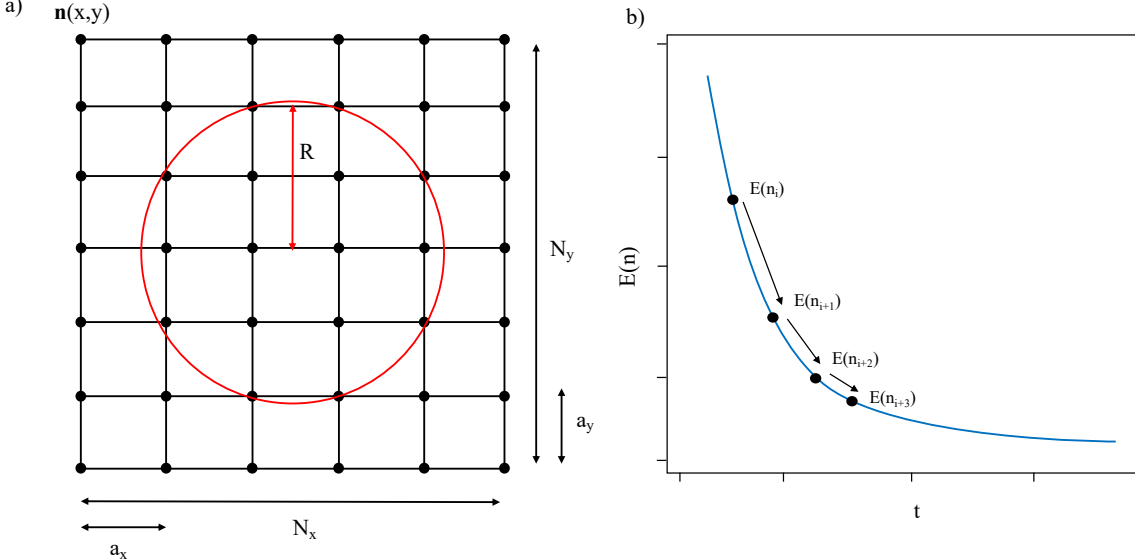


Figure 7: **a)** Grid setup, the director field $\mathbf{n}(x, y)$ is defined on each grid point with its orientation restricted to $\mathbf{n} = \mathbf{e}_z$ anywhere outside the red circle. **b)** Gradient descent, at each step \mathbf{n} updated proportionally to $-\delta E / \delta \mathbf{n}$ and therefore, energy finds a local minima.

$$\mathbf{n}_{i+1} = \mathbf{n}_i - \gamma \Delta t \frac{\delta E}{\delta \mathbf{n}} \quad (2.3)$$

Where γ is the learning rate and Δt is the time step⁸, thus, we record an ‘evolution’ of \mathbf{n} with respect to time, Fig. 7b. Note \mathbf{n} is normalised at each step. To numerically calculate $\delta E/\delta \mathbf{n}$ eq.(2.1) the curl and Laplacian are computed using finite difference methods:

$$\frac{\partial n_\mu}{\partial x} = \frac{n_\mu^{i+1,j} - n_\mu^{i-1,j}}{2a_x} \quad (2.4)$$

$$\frac{\partial^2 n_\mu}{\partial x^2} = \frac{n_\mu^{i+1,j} - 2n_\mu^{i,j} + n_\mu^{i-1,j}}{a_x^2} \quad (2.5)$$

Where $\mu \in \{x, y, z\}$ and i, j represents a grid point. It is here we enforce our circular boundary conditions;

$$\Delta \mathbf{n}(x, y) \begin{cases} = \mathbf{0} & x^2 + y^2 > R^2 \\ \in \mathbb{R}^3 & \text{otherwise} \end{cases} \quad (2.6)$$

ensuring throughout the minimisation, $\mathbf{n}(x, y)$ outside the circle has a ‘constrained’ orientation equal to its original value $\mathbf{n} = -\mathbf{e}_z$.

2.1.1 Limitations

The proposed method has three fundamental limitations worth mentioning; i) stopping criteria ii) computation time iii) discontinuity.

i) Defining an effective stopping criteria is a well-known limitation of gradient descent, with many possible solutions. In our case we use a simple criteria;

$$\Delta E(\mathbf{n}) < \sigma$$

where σ is a pre-set tolerance level. This method itself is limited, particularly due to the possibility of a premature stop, a problem advanced methods often look to address [35]. Since we only run a handful of simulations, it is reasonable to address this problem by both qualitatively studying energy against time plots and running the simulation for an additional series of steps once the condition is met.

ii) In the majority of cases our simulations are short, thus, the limitation on computation time induced by eq.(2.3) is somewhat irrelevant. However, it is important to note the time complexity with respect to grid size N , $\mathcal{O}(N^2)$. In some cases we employ a variable (decaying) learning rate;

$$\gamma_t = \gamma_0 + \frac{\lambda}{1 + t\tau} \quad (2.7)$$

where λ and τ are decay constants, and γ_0 is a ‘base’ learning rate. Importantly, this method is used with caution due to the possible amplification of limitation iii). It will be mentioned explicitly when used.

⁸‘Leaning rate’ is a term coined in the field of machine learning, an important application of gradient descent. I use the term here as it remains descriptive of its function outside of this context [34].

iii) In section 1.2.1 it is stated topological charge is conserved under *continuous* transformations of the director. Numerically, it is impossible to perform such transformations and due to the complexity $\mathcal{O}(N^2)$ we will not reach quasi-continuity. Although discontinuity limits the physical accuracy of our system, it generates an area of analysis. Hence, the affect of grid size N is studied in-depth.

2.1.2 Additional Information

Throughout our analysis we consider a real system projected onto an the NxN grid (Fig. 7a). This is named the effective system, where effective energy E_e and effective constants K_e and B_e differ from their respective real space values. Since B is the primary independent variable, it is useful to convert between B and B_e using the following formula;

$$B_e = \frac{BL}{KNa} \quad (2.8)$$

where L is the width (and height) of the real system. Energy may also be converted:

$$E_e = \frac{E}{K} \quad (2.9)$$

3 Results and Discussion

3.1 Pilot Simulation

Initially, the minimum energy states of a simple $Q = +1, \pi$ twisted skyrmion were measured. The minimisation eq.(2.1) is performed with a constant effective elastic constant $K_e = 1$ and effective B values ranging from 0.1 – 1.2. A full list of simulation parameters is given in table 2, note the diameter D of our skyrmion eq.(2.2) and circular constraints eq.(2.6) is 50 grid points. We observe a systematic deviation from the expected energy against B relationship, primarily due to the introduction of the HH instability, Fig 8 shows such observations.

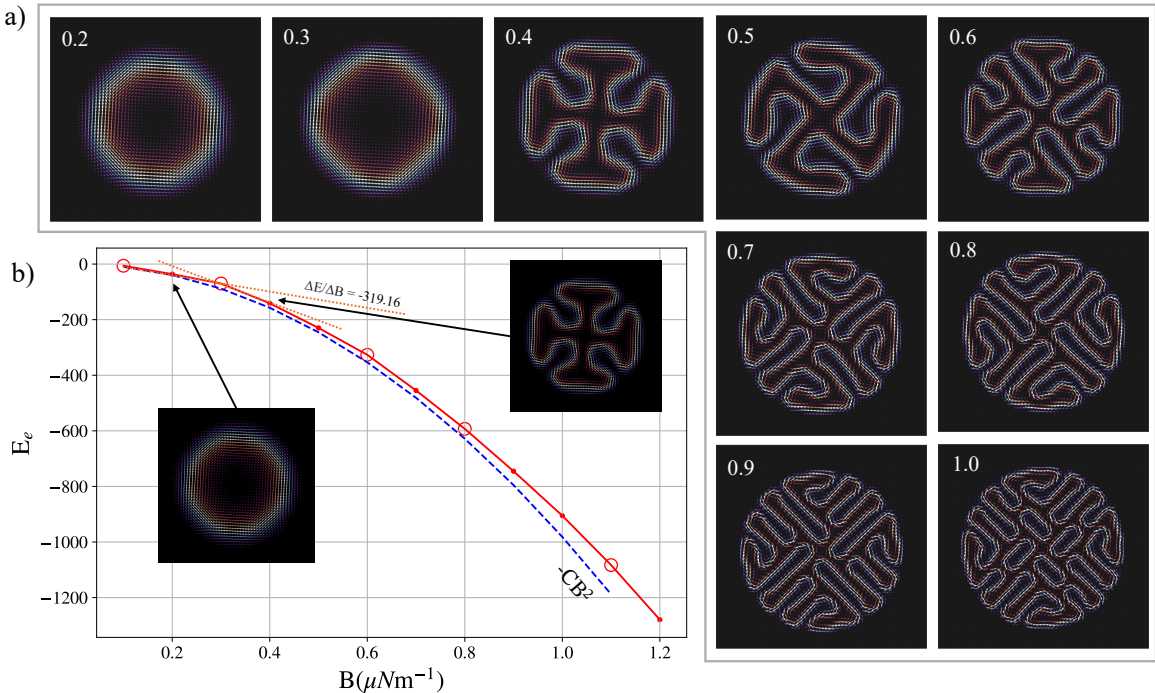


Figure 8: **a)** The final states of skyrmions initialised using eq.(2.2) and minimised via gradient descent eq.(2.3) under circular boundary conditions eq.(2.6). Each state is labeled by its effective B_e **b)** Effective energy E_e against B_e , the blue dashed line denotes $-CB^2$ represents the expected relationship eq.(1.13) and observed values are in red. Refer to table 4 for the data used.

At first sight, although the structures demonstrate some un-clear complexities, the HH instability is clear. The number of undulations is related to B, increasing in discrete steps; 0, 4, 8, 12 etc. This behaviour can be predicted analytically by making a naive approximation and comparing the diameter D to the preferred length scale p ($p = 2\pi/q_0$, $q_0 = B/K$), where the expected number of undulations U_E is given by;

$$U_E = 2 \cdot \text{floor}\left(\frac{D}{p}\right) \quad (3.1)$$

i.e. twice the maximum number of full 2π rotations with wavelength p that ‘fit’ across the diameter of the circle. Fig. 9 demonstrates how this is approximately equal to the number of expected undulations.

This simple model performs at a surprisingly high degree of accuracy, thus, the observations highlight; i) the systems strong tenancy to align with ground state pseudo layers, twisting 2π on a length scale p under circular boundary conditions that mis-align drastically. ii) Jumps in the number of undulations at $D \approx np$.

B_e	U_e	U_o
0.2	0	0
0.3	4	0
0.4	4	4
0.5	4	4
0.6	8	8
0.7	8	8
0.8	12	8
0.9	12	12
1.0	12	12

Table 1: A table to show the results of eq.(3.1), U_e is the expected number of undulations, U_o is observed. For p and D/p values refer to table 3.

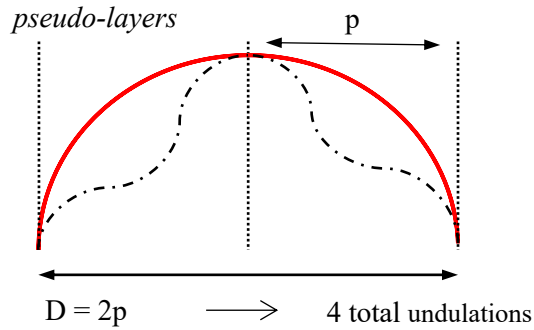


Figure 9: Demonstration of how undulations can arise under circular boundary conditions, thus, eq(3.1) makes a reasonable approximation.

These discrete jumps have energetic significance observed as a ‘stepping’ E against B gradient ($\Delta E/\Delta B$), Fig. 8b. Energy drops toward the expected relationship at each structural change (introduction of additional undulations), where the geometry of the boundary conditions align (as closely as possible) with the geometry of the ground state. The steps in gradient ($\Delta E/\Delta B$) are most prominent at larger length scales (lower B), which may be expected, Fig. 10a: When the magnitude of preferred length scale relative to the size of system is reduced, structural changes are smaller, having less influence of the systems energy functional eq.(1.7, 1.10). Additional evidence is provided via analysis of the skyrmions perimeter, where a jump in perimeter length is prominent for the initial, large-scale structural change and almost indistinguishable at higher values of B , Fig. 10b.

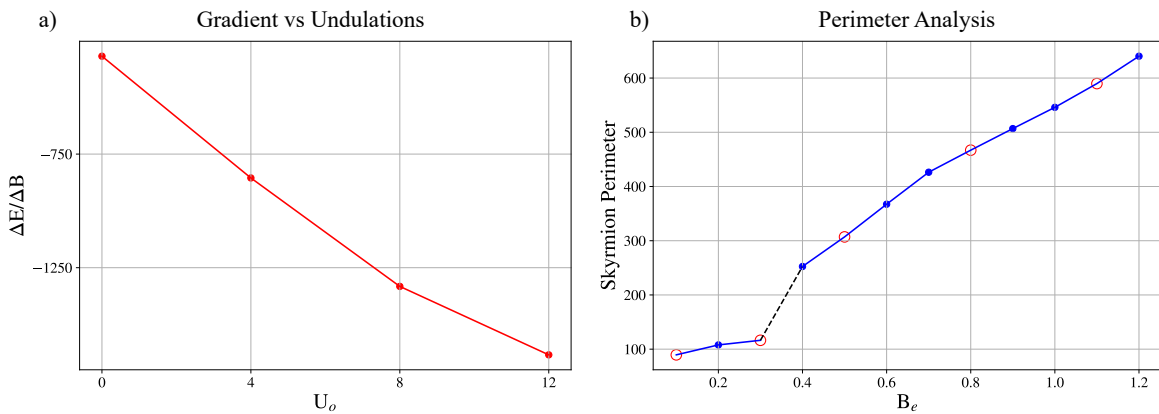


Figure 10: **a)** The gradients of E vs B (Fig. 8b) where the number of undulations stays constant. **b)** The perimeter of each skyrmion in its final state against B_e . Again, red circles represent B_e values where number of undulations changes.

We can interpret this behaviour as a sudden relief of frustration via the HH instability, best depicted by the evolution of the skyrmion under energy minimisation, given by Fig. 12 and supplementary video A.

As of now, we have suggested an introduction of *symmetric* undulations as the skyrmion relieves frustration via the HH instability. The final states presented (Fig. 8a) show a number of additional complexities, notably at $B_e = 0.5$ and $B_e = 1.0$. The (somewhat disturbing) $B_e = 0.5$ final state demonstrates important structural behaviour; the skyrmion exhibits periodicity at preferred length scales perpendicular to each-other. Since the circular boundary conditions never align with the ground state and all the rotated variants eq.(1.12), the skyrmion appears to find stability under a complex superposition of 2π rotations of the director in multiple directions. Where rotations are most stable over multiples of the preferred length scale np . This is made explicitly clear quantitatively, by taking the fast fourier transform of $n_z(x, y)$.

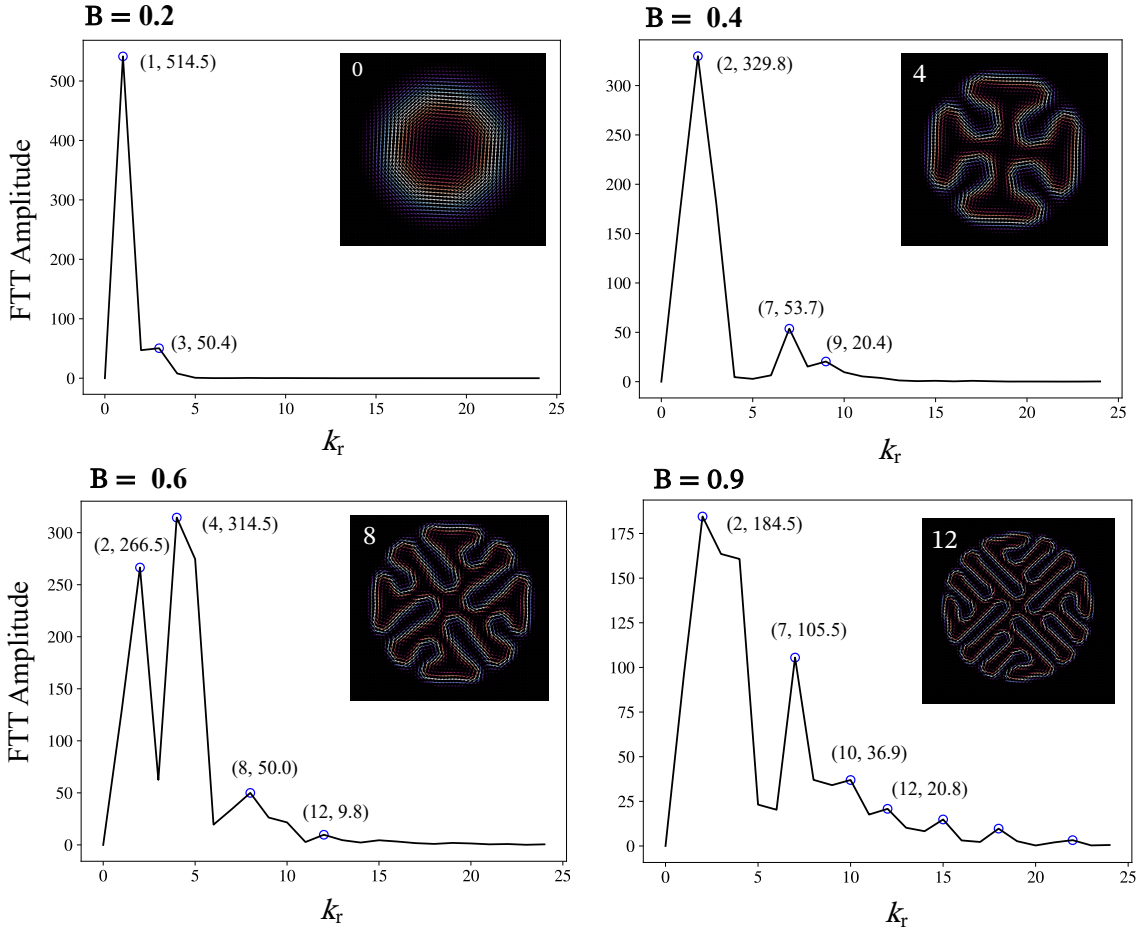


Figure 11: The FFT of $n_z(x, y)$. Given for four states, each with a different total number of undulations. The most prominent peaks are marked with a blue circle and a co-ordinate (k_r , Amplitude). At large B values, where the preferred length scale p is small, skyrmions exhibit a superposition of length scales.

Each peak represents a length scale, as B increases more peaks take shape. Following the previous discussion, consider the case where $B_e = 0.9$ with $D/p \approx 7.16$, it is possible for rotations of n_z to occur

over length scales $p, 2p, \dots, 6p$ across the skyrmions diameter, thus, many additional peaks are observed. We note that, where numerous ‘allowed’ length-scales are present, stable states grow in complexity (extensive superposition of ground states) and their structural behaviour is less predictable. Recall the E_e vs B_e relationship (Fig. 8b), the ‘tail off’ observed at higher values of B seems to correspond to this enforced inability (boundary conditions) to reach any given ground state, the system finds a complex superposition of the most favourable length scales but can never reach a perfect ground state.

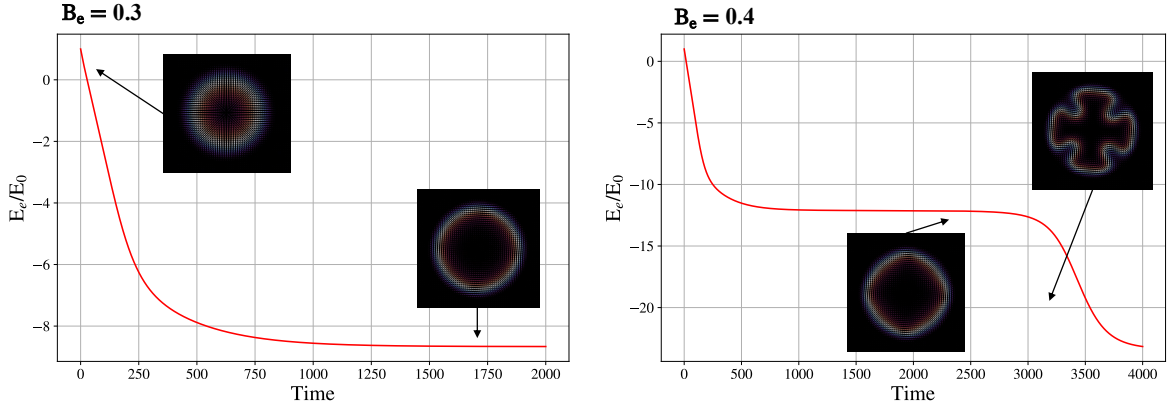


Figure 12: The evolution of skyrmion energy against time t eq.(2.3) for $B_e = 0.3$ and 0.4 , these plots aim to demonstrate the sudden release of frustration when HH undulations are introduced (supplementary video A). E_0 is the value of effective energy at the start of the simulation.

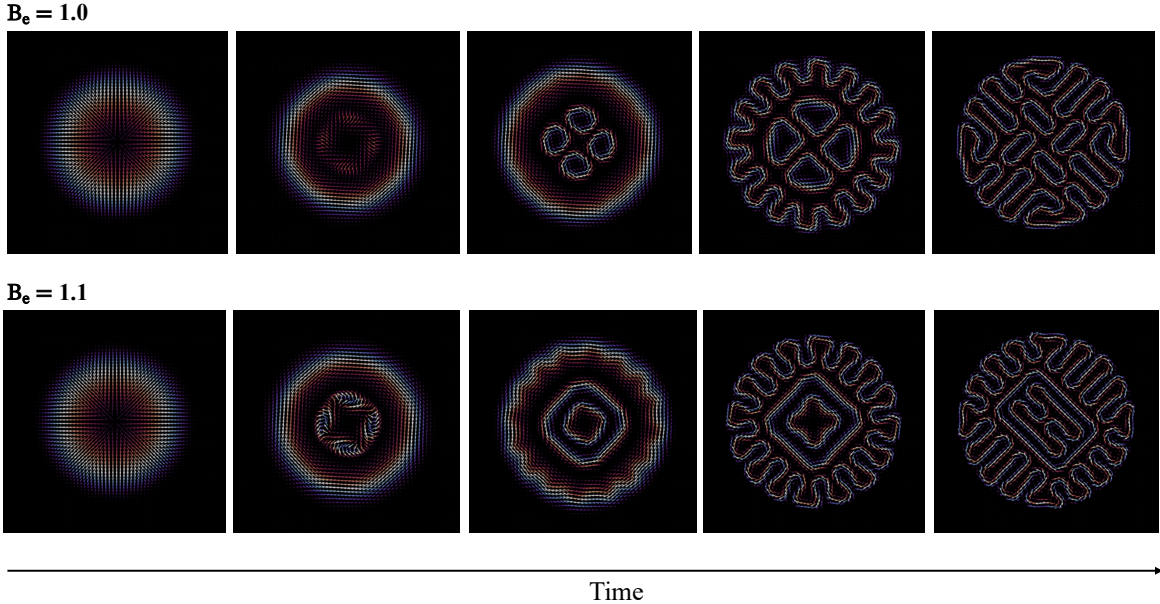


Figure 13: Supplementary video B, The evolution of skyrmions under energy minimisation eq.(2.1) where $B_e = 1.0$ and 1.1 . Importantly these observations show a change in topology.

In search of stability, the $B_e = 1.0$ state appears to have undergone a topological change from $Q = +1$ to $Q = -3$ ($+1 - 4$), it is reasonable to assume, this is a consequence of the small grid size $N = 50$

and therefore, preferred length scales reach a similar magnitude to grid separation a .

This change is demonstrated by Fig. 13 and supplementary video B, where the evolution of the skyrmion at $B = 1.0$ and 1.1 is shown. Interestingly, we see the topological change is introduced prior to the introduction of undulations, suggesting, if possible, this change is preferred. Note the transition from a π to 3π twisted skyrmion in the $B = 1.1$ case, although this change is prohibited in continuous systems (requires a singularity) topological charge is conserved⁹. This behaviour is better understood by considering systems with larger grid sizes.

3.2 Varied grid size

Again, we measure the evolution and minimum energy states of a $Q = +1, \pi$ twisted skyrmion. However, in this case the effect of grid size N on structural behaviour is considered. Since B_e is dependant on N eq.(2.8), throughout this section real-space B values ranging from $1.625 - 19.5 \mu\text{Nm}^{-1}$ are used for a direct comparison (equivalent to $B_e = 0.1 - 1.2$ when $N = 50$). The key observation here is the introduction of additional twists ($\pi \rightarrow 3\pi \rightarrow 5\pi$) during minimisation, these twists are introduced at lower B when N is increased. A selection of final states are compared in Fig. 14.

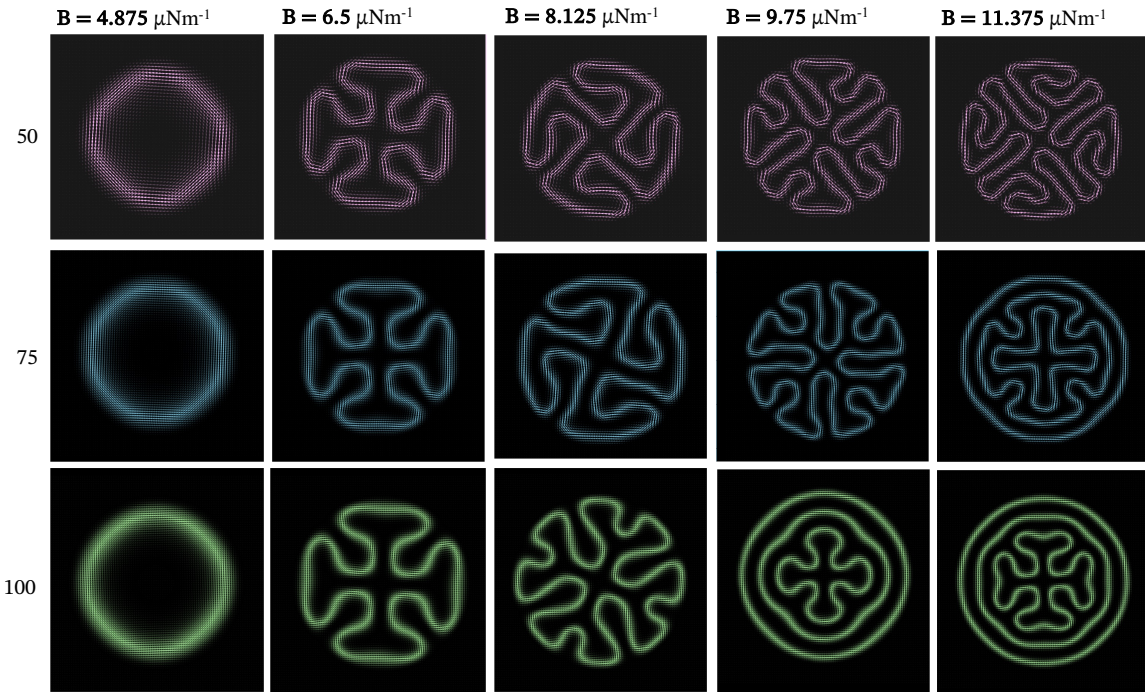


Figure 14: Final states of skyrmions where minimisation eq.(2.2, 2.3, 2.6) is run with increasing grid sizes. Each column has the same B value and each row has the same grid size. For respective B_e values and preferred length scales refer to table 3.

Immediately we gain information to aid our previous discussion. Observations at lower B solidify the idea of frustration release via the HH instability as the skyrmion seeks a preferred length scale. We see discrete jumps in the number of undulations as described, reinforced by the stepping gradient

⁹odd twisted skyrmions have $|Q| = 1$

observed for all grid sizes between $B = 4.875 - 6.5 \mu\text{Nm}^{-1}$, see Fig. 15a. Prior to the introduction of an additional twist at $B = 9.75 \mu\text{Nm}^{-1}$ ($B_e^{50} = 0.5$), the first set of differentiating behaviour is observed: As N is increased the ‘perpendicular superposition’ is removed and symmetric undulations appear. Note that superposition of length scales is still present, though it is done in such a way to retain symmetry. Such observations suggest this behaviour is a direct consequence of low grid size, where systems are unable to ‘find’ a symmetric local minima and thus resort to an anti-symmetric superposition. Therefore, we make the following hypothesis regarding the nature of our system: As a skyrmion minimises its energy, under the circular boundary presented, it has both a preference for a length scale on which it twists ($p = 2\pi/q_0$ to satisfy $\mathbf{n} \cdot \nabla \times \mathbf{n} = -q_0$) and a preference for symmetry. This symmetry preference is exemplified by the introduction of an additional twist. In a sense, this is the most symmetric structural change possible. Studying the energy evolution provides additional insight, showing the addition of a twist allows the system to avoid a plateau in energy minimisation thus releasing frustration more efficiently than the HH instability. Eventually, the system is able to reach a final state with a lower effective energy E_e closer to the expected relationship.

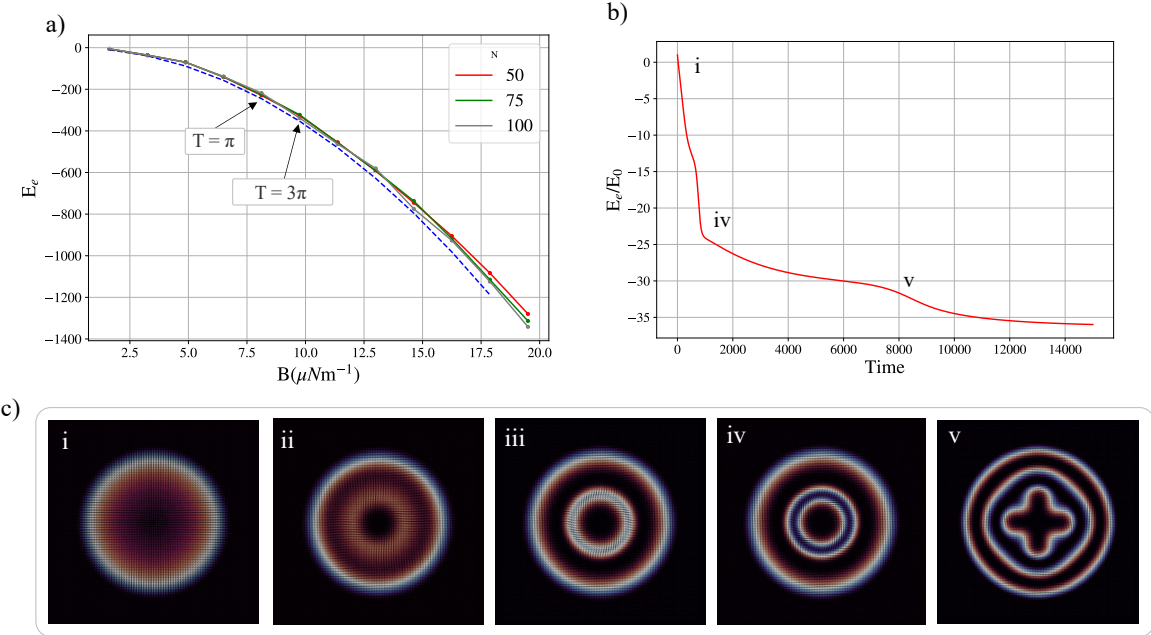


Figure 15: **a)** Effective energy E_e against B for grid sizes set to 50, 75 and 100. The twist T of two final states where $N = 100$ is marked, aiming to show where twist is introduced at high N , the skyrmions energy gets closer to the helical ground state. **b, c)** The evolution of a skyrmion where $N = 100$ and $B = 9.75 \mu\text{Nm}^{-1}$. The twist causes a rapid decrease in energy, this evolution is represented by supplementary video C.

Although the hypothesis above explains, to some extent, why the system wants to twist, it does not describe the mechanism. In the previous section it was assumed topology was altered as a consequence of small grid size, here we observe the complete opposite. The functional eq.(1.10) and minimisation methodology eq.(2.3) considers the global state of the skyrmion at each time step, though it is reliant on the difference between the director \mathbf{n} at each grid point (finite difference methods, eq.(2.4, 2.5)). Our observations show, when the system gets *closer* to continuity the geometric constraints influence global,

topological frustration¹⁰. This topological frustration is released locally at the radial point where a new twist is introduced¹¹ (Fig. 15c, supplementary video C). Recall, a change of winding number is prohibited at complete continuity (1.2.1), here the $N = 100$ system is still far from continuity and gradient descent is able to surpass the ‘energetic barrier’ required to introduce a twist. Since similar behaviour is observed at large B for small N , global frustration appears to be induced by some combination of continuity (ensuring dominant collective behaviour) N and the size of the desired length scale; where smaller length scales increase both global and local frustration. Notice, in Fig. 15c(v), the ‘inner π twisted skyrmion’ obtains a small radius relative to the size of the preferred length scale, local geometric effects are dominant and frustration is released by the HH instability as discussed (i.e. stability is reached using a combination of both mechanisms).

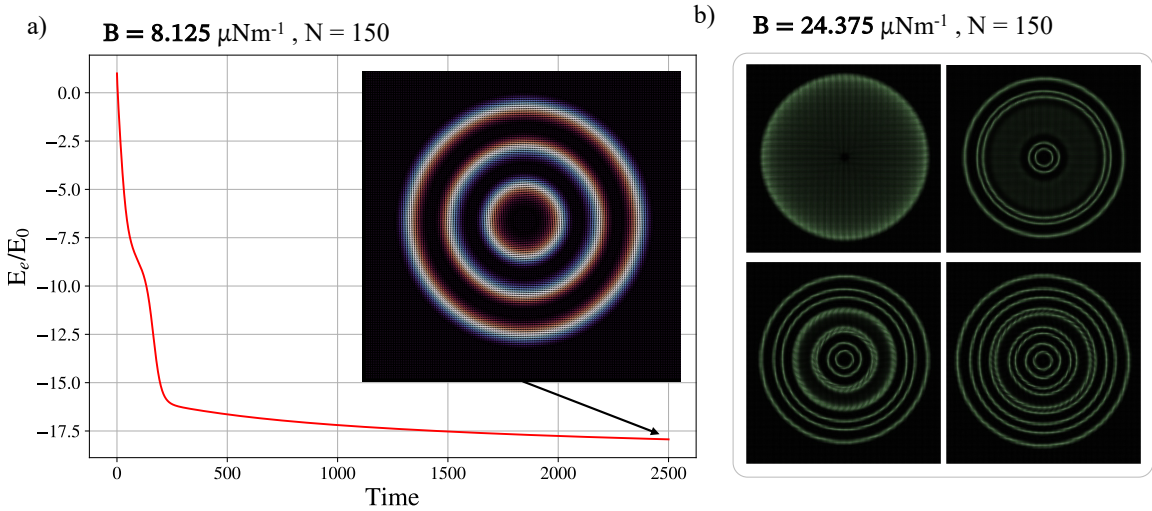


Figure 16: Skyrmion evolution under circular boundary conditions **a)** Energy evolution and final state when $B = 8.125 \mu\text{Nm}^{-1}$ and $N = 150$. **b)** State evolution when $N = 150$ at high B . Multiple twists are introduced, see supplementary video D.

A natural progression is to carry out further study at larger N , showing a scenario where the HH instability is avoided entirely, even at low B . Due to the time complexity limitation $\mathcal{O}(N^2)$, we ran a limited number of tests choosing those expected to provide the most value. A variable learning rate was also employed eq.(2.7) with $\gamma_0 = 2$ and $\tau = 0.01$. Two examples are given (Fig. 16); When $B = 8.125 \mu\text{Nm}^{-1}$ the skyrmion is minimised to an almost perfect 3π twisted state. Un-like previous examples there is no evidence of the HH instability, demonstrating where N is large and $p < D/3$ the twisting mechanism is favoured. The evolution of the skyrmion with a much higher of $B = 24.375 \mu\text{Nm}^{-1}$ was also ran showing the the emergence of many twists prior to evidence of undulations (supplementary video D).

¹⁰‘In general, topological defects result from system frustration that can arise from either local geometrical effects, i.e., geometrical frustration, or global geometrical effects, i.e., topological frustration.’ [2]

¹¹‘Topological frustration needs to be solved somewhere; geometrical frustration has to be solved everywhere.’ [2]

3.3 $n\pi$ Twisted Skyrmions

The observations made in the previous section are reinforced by studying skyrmions initialised with a 3π and 5π twist ($N = 100$). For both cases a new definition of ψ eq.(2.2) is required, the definition for a 3π twisted skyrmion is given:

$$\psi = \frac{(|x + iy|^2 - R^2)(|x + iy|^2 - (\frac{R}{3})^2)\alpha e^{i\theta}}{(x - iy)(|x + iy|^2 - (\frac{2R}{3})^2)} \quad (3.2)$$

Notice this ensures $\mathbf{n} = -\mathbf{e}_z$ at $R/3$ and R , $\mathbf{n} = \mathbf{e}_z$ at $2R/3$. Small B values equal to those in Fig. 14 ($4.875 - 11.375 \mu\text{Nm}^{-1}$) are considered. We provide a short demonstration minimisation, with particular interest in scenarios where preferred length scale is larger than the wavelength of twist, $p > D/3$ (3π) or $p > D/5$ (5π). This situation, alongside the $3\pi/5\pi$ initial states is shown in Fig. 17.

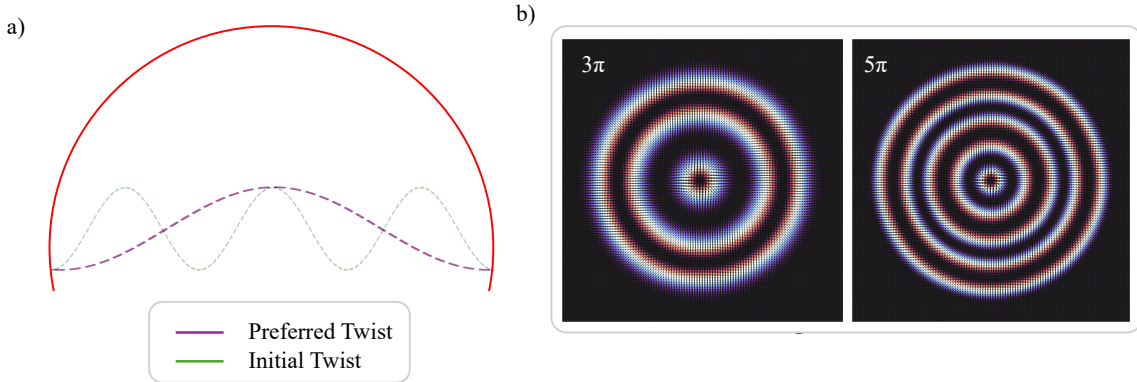


Figure 17: **a)** A diagram to show a scenario in which the preferred length scale p is longer than the wavelength of initial twist. **b)** The initial states considered in this section, the skyrmion twists a total of 3π (left) or 5π (right) along its radius.

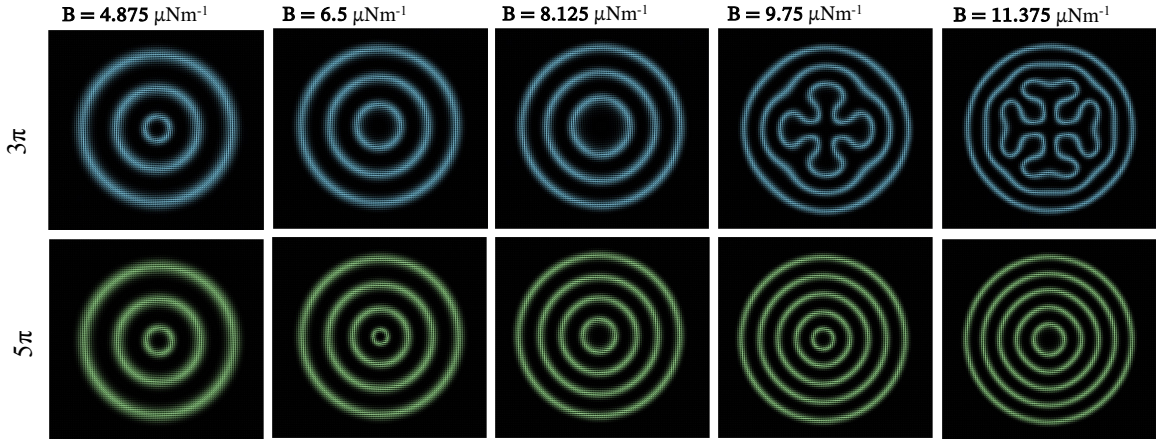


Figure 18: Final states of 3π and 5π skyrmions minimised under circular confinement eq.(2.2, 2.3, 2.6). Each column has the same B value and each row has the same initial twist. Key observations are i) the vanishing twist when the skyrmion is initialised with a 5π twist, ii) energy very close to the ground state (table 4).

The final states, shown in Fig. 18 align well with previous observations and hypotheses. The system, particularly in the 5π case, is able to satisfy the length scale and symmetry preference without the introduction of undulations. As seen in the previous section where $N = 150$, twist is the favourable mechanism for minimisation. When $B = 4.875\mu\text{Nm}^{-1}$ or $6.5\mu\text{Nm}^{-1}$ and initial twist is 5π , a collapse or *vanishing* of twist is observed as a consequence of the scenario presented Fig. 17a. Prior research has observed similar phenomena where a free (no enforced boundary conditions) 6π twisted skyrmion collapses to a π twisted skyrmion. The authors (Foster *et al*) make the following relevant statement; '*the central skyrmion contracts due to the accumulative pressure from each exterior skyrmion ring.*' [11]. In this case, we observe an analogous effect. Outer rings spread out to meet the desired length scale, inducing pressure on the central skyrmion leading to its removable.

Fig. 20 shows the collapse when $B = 4.875\mu\text{Nm}^{-1}$ in detail. The energy against time profile (Fig. 20b) is particularly striking due to the slow rising energy under gradient descent. This behaviour is not completely clear (an area for further exploratory study), however, note the following observation: In the referenced situation [11], where the skyrmion is unconstrained, radius of outer skyrmion rings decreases throughout the collapse, thus ensuring a constant downward energy trajectory. Here, it seems the boundary conditions deny such simplicity and stability is found at a larger energy where $\mathbf{n} \cdot \nabla \times \mathbf{n}$ is closer to $-q_0$.

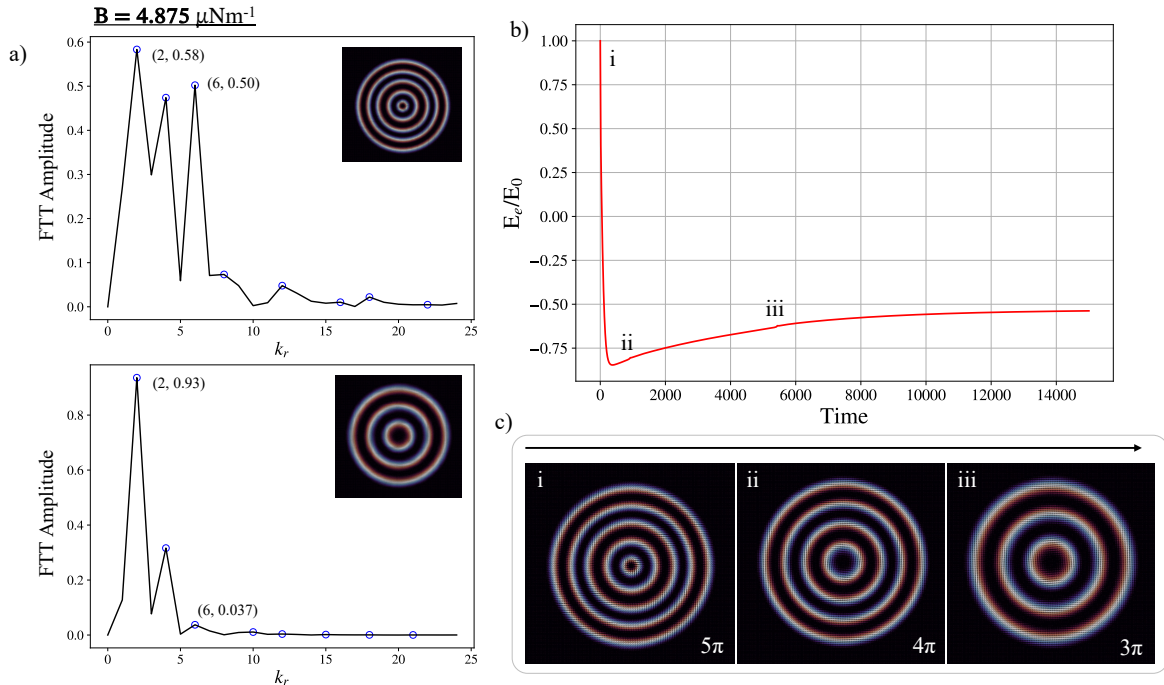


Figure 19: The collapse of 5π to 3π twist under minimisation. **a)** The FFT of $n_z(x, y)$ showing the removable of length scales. **b, c)** The energy and state evolution over time, a dramatic drop followed by smooth rising in energy is observed as twist is removed, twist is eventually stabilised. Supplementary video E compares this evolution to observations made by Foster *et al* [11]

The collection of observations made leads us to our last conclusion: Circular boundary conditions (to a limited extent) stabilise twist. Noting in the given example Fig. 20, $D/p \approx 2.39$ though a 3π twist is

stable. The limits of twist stability are tested when the Fig. 17a scenario is extremised, a 7π twisted skyrmion was simulated with $B = 1.625 \mu\text{Nm}^{-1}$ ($D/p \approx 0.80$). We observe a smooth removal of twist leaving a seemingly topologically protected core, preventing the final state from exhibiting even a full π twist.

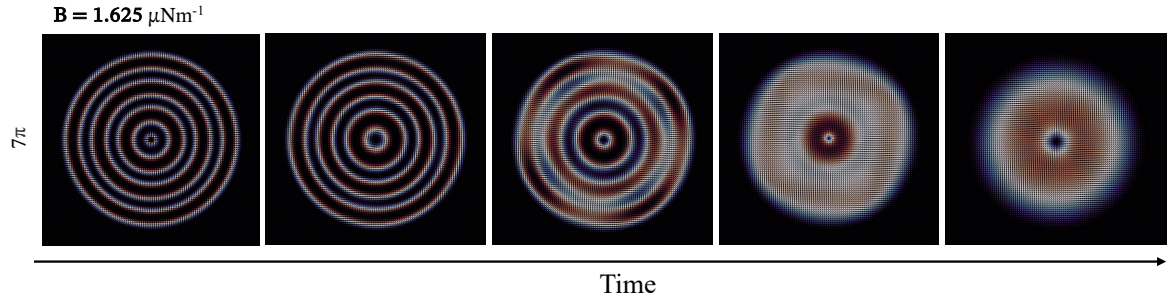


Figure 20: Supplementary video F, the smooth removable of twist when Fig. 17a is extremised. The skyrmion is initialised with a 7π twist and $B = 1.625 \mu\text{Nm}^{-1}$.

4 Conclusion

The diversity of skyrmion topology and structural dynamics presents opportunity for a broad range of exploratory study. Here, using computational simulations, we have investigated the effects of constraining orientation of the director \mathbf{n} at the skyrmions boundary. Such conditions prevent the director \mathbf{n} from reaching the desired ground state eq.(1.12) (where $\mathbf{n} \cdot \nabla \times \mathbf{n}$ is satisfied) and therefore frustration is induced. Two key frustration release mechanisms were identified: Where local geometric frustration is dominant (at low B and grid size N), the Helfrich-Hurault (HH) instability is observed. The skyrmion undulates in such a way to ensure \mathbf{n} twists on a length scale p and thus, the skyrmion exhibits a complex superposition of length scales $\approx np$ to reach stability.

When grid size N is increased and preferred length scale p is reduced, the enforced circular boundary condition induces global frustration, released via the introduction of a 2π twist ($\pi \rightarrow 3\pi$). The resulting twisted skyrmions better satisfy $\mathbf{n} \cdot \nabla \times \mathbf{n} = -q_0$ and thus, where possible (i.e. where boundary conditions have global influence), the introduction of a twist is favoured over the HH instability. Such observations lead us to the following hypothesis; ‘As a skyrmion minimises its energy, under the circular boundary presented, it has both a preference for a length scale on which it twists and a preference for symmetry’. Additional simulations, where twist was pre-introduced (wavelength λ_t), aligned well with prior observations. Showing vanishing twist where preferred length scale $p \gg \lambda_t$ and stabilisation of twist at $p \approx \lambda_t$.

4.1 Further Work

Although the direct application of presented results is not clear, these observations may influence additional confined skyrmion research, leading to important uses in spintronics or display systems. The demonstrated stabilisation of twist presents opportunity for further investigation: The limitations of twist stability could be analysed in more detail, developing a precise qualitative understanding of

when twists stabilises with respect to the preferred length scale and boundary condition geometry. Studying high degree $|Q| > 1$ skyrmions may provide additional insight, noting their stability and effect on the described frustration release mechanisms.

References

- [1] R. D. Kamien and J. V. Selinger, “Order and frustration in chiral liquid crystals,” *Journal of Physics: Condensed Matter*, vol. 13, no. 3, p. R1, 2001.
- [2] C. Blanc, G. Durey, R. D. Kamien, T. Lopez-Leon, M. O. Lavrentovich, and L. Tran, “Helfrich-hurault elastic instabilities driven by geometrical frustration,” *Reviews of Modern Physics*, vol. 95, no. 1, p. 015004, 2023.
- [3] S. Mühlbauer, B. Binz, F. Jonietz, C. Pfleiderer, A. Rosch, A. Neubauer, R. Georgii, and P. Boni, “Skyrmion lattice in a chiral magnet,” *Science*, vol. 323, no. 5916, pp. 915–919, 2009.
- [4] X. Yu, Y. Onose, N. Kanazawa, J. H. Park, J. Han, Y. Matsui, N. Nagaosa, and Y. Tokura, “Real-space observation of a two-dimensional skyrmion crystal,” *Nature*, vol. 465, no. 7300, pp. 901–904, 2010.
- [5] A. Nych, J.-i. Fukuda, U. Ognysta, S. Žumer, and I. Mušević, “Spontaneous formation and dynamics of half-skyrmions in a chiral liquid-crystal film,” *Nature Physics*, vol. 13, no. 12, pp. 1215–1220, 2017.
- [6] N. S. Kiselev, A. Bogdanov, R. Schäfer, and U. Rößler, “Chiral skyrmions in thin magnetic films: new objects for magnetic storage technologies?” *Journal of Physics D: Applied Physics*, vol. 44, no. 39, p. 392001, 2011.
- [7] A. Fert, V. Cros, and J. Sampaio, “Skyrmions on the track,” *Nature nanotechnology*, vol. 8, no. 3, pp. 152–156, 2013.
- [8] F. N. Rybakov and N. S. Kiselev, “Chiral magnetic skyrmions with arbitrary topological charge,” *Physical Review B*, vol. 99, no. 6, p. 064437, 2019.
- [9] M. Hassan, S. Koraltan, A. Ullrich, F. Bruckner, R. O. Serha, K. V. Levchenko, G. Varvaro, N. S. Kiselev, M. Heigl, C. Abert *et al.*, “Dipolar skyrmions and antiskyrmions of arbitrary topological charge at room temperature,” *Nature Physics*, pp. 1–8, 2024.
- [10] J. Eun, J. Pollard, S.-J. Kim, T. Machon, and J. Jeong, “Layering transitions and metastable structures of cholesteric liquid crystals in cylindrical confinement,” *Proceedings of the National Academy of Sciences*, vol. 118, no. 33, p. e2102926118, 2021.
- [11] D. Foster, C. Kind, P. J. Ackerman, J.-S. B. Tai, M. R. Dennis, and I. I. Smalyukh, “Two-dimensional skyrmion bags in liquid crystals and ferromagnets,” *Nature Physics*, vol. 15, no. 7, pp. 655–659, 2019.
- [12] J. H. Han, *Skyrmions in condensed matter*. Springer, 2017, vol. 278.
- [13] B. Mendelson, *Introduction to topology*. Courier Corporation, 1990.

- [14] T. Lancaster, “Skyrmions in magnetic materials,” *Contemporary Physics*, vol. 60, no. 3, pp. 246–261, 2019.
- [15] B. Senyuk, Q. Liu, S. He, R. D. Kamien, R. B. Kusner, T. C. Lubensky, and I. I. Smalyukh, “Topological colloids,” *Nature*, vol. 493, no. 7431, pp. 200–205, 2013.
- [16] F. Canfora and S. C. Rebolledo-Caceres, “Skyrmions at finite density,” *Modern Physics Letters A*, vol. 38, no. 12n13, p. 2330002, 2023.
- [17] J. Hagemeister, A. Siemens, L. Rózsa, E. Y. Vedmedenko, and R. Wiesendanger, “Controlled creation and stability of $k \pi$ skyrmions on a discrete lattice,” *Physical Review B*, vol. 97, no. 17, p. 174436, 2018.
- [18] A. Bogdanov and A. Hubert, “The stability of vortex-like structures in uniaxial ferromagnets,” *Journal of magnetism and magnetic materials*, vol. 195, no. 1, pp. 182–192, 1999.
- [19] S. Sachdev, “Quantum phase transitions,” *Physics world*, vol. 12, no. 4, p. 33, 1999.
- [20] P. Toledano and J.-c. Toledano, *Landau Theory Of Phase Transitions, The: Application To Structural, Incommensurate, Magnetic And Liquid Crystal Systems*. World Scientific Publishing Company, 1987, vol. 3.
- [21] C. A. Gonano, R. E. Zich, and M. Mussetta, “Definition for polarization p and magnetization m fully consistent with maxwell’s equations,” *Progress In Electromagnetics Research B*, vol. 64, pp. 83–101, 2015.
- [22] M. Orchin, R. S. Macomber, A. R. Pinhas, and R. M. Wilson, *The vocabulary and concepts of organic chemistry*. John Wiley & Sons, 2005, ch. 1. Atomic Orbital Theory.
- [23] E. Merzbacher, *Quantum mechanics*. John Wiley & Sons, 1998, p. 372–373.
- [24] P. W. Anderson, “Theory of magnetic exchange interactions: exchange in insulators and semiconductors,” in *Solid state physics*. Elsevier, 1963, vol. 14, pp. 99–214.
- [25] N. Nagaosa and Y. Tokura, “Topological properties and dynamics of magnetic skyrmions,” *Nature nanotechnology*, vol. 8, no. 12, pp. 899–911, 2013.
- [26] S. Bhowal, S. Satpathy, and P. Sahu, “Magnetic skyrmions in condensed matter physics,” *arXiv preprint arXiv:2005.07635*, 2020.
- [27] P. J. Ackerman, R. P. Trivedi, B. Senyuk, J. van de Lagemaat, and I. I. Smalyukh, “Two-dimensional skyrmions and other solitonic structures in confinement-frustrated chiral nematics,” *Physical Review E*, vol. 90, no. 1, p. 012505, 2014.
- [28] G. W. Gray, “Molecular structure and the properties of liquid crystals,” (*No Title*), 1962.
- [29] L. W. T. Kelvin, *Baltimore lectures on molecular dynamics and the wave theory of light*. CUP Archive, 1904.
- [30] I. Dierking, “Chiral liquid crystals: structures, phases, effects,” *Symmetry*, vol. 6, no. 2, pp. 444–472, 2014.

- [31] S. Goshen, D. Mukamel, and S. Shtrikman, “Application of the landau theory of phase transitions to liquids-liquid crystals transitions,” *Solid State Communications*, vol. 9, no. 10, pp. 649–652, 1971.
 - [32] P.-G. De Gennes and J. Prost, *The physics of liquid crystals*. Oxford university press, 1993, no. 83, ch. 3.1.3.2 The one-constant approximation.
 - [33] C. Jin, C. Zhang, C. Song, J. Wang, H. Xia, Y. Ma, J. Wang, Y. Wei, J. Wang, and Q. Liu, “Current-induced motion of twisted skyrmions,” *Applied Physics Letters*, vol. 114, no. 19, 2019.
 - [34] K. P. Murphy, *Machine learning: a probabilistic perspective*. MIT press, 2012.
 - [35] K. Rao, P. Malan, and J. B. Perot, “A stopping criterion for the iterative solution of partial differential equations,” *Journal of Computational Physics*, vol. 352, pp. 265–284, 2018.
 - [36] T. Machon and G. P. Alexander, “Umbilic lines in orientational order,” *Physical Review X*, vol. 6, no. 1, p. 011033, 2016.
-

5 Appendix

5.1 A: Derivations

5.1.1 A.1 Spin Hamiltonian in the Continuum Limit

Recall the Hamiltonian:

$$H = J \sum_{i,j} \mathbf{S}_i \cdot \mathbf{S}_j + \sum_{i,j} \mathbf{D}_{i,j} \cdot (\mathbf{S}_i \times \mathbf{S}_j) \quad (5.1)$$

Now consider a 2D simple cubic bravais lattice with lattice spacing a . By taking the limit $a \rightarrow 0$ and $N \rightarrow \infty$, \mathbf{S}_i can be related to an infinitesimally small chunk of a director field $\mathbf{n}(x, y)$ given by its gradient $\partial_k \mathbf{n}$, $k \in \{x, y, z\}$. Therefore the first term of the Hamiltonian becomes;

$$J \sum_{i,j} \mathbf{S}_i \cdot \mathbf{S}_j \rightarrow \int \frac{J}{2} \sum_k \partial_k \mathbf{n} \cdot \partial_k \mathbf{n} \, dx dy$$

where a factor of $\frac{1}{2}$ is introduced to account for repeated terms.

Taking the second (DMI) term into the continuum limit is complex and not intuitive. However, qualitatively we expect the term to represent the relative orientation of magnetic moments. In continuous systems this is given by the curl:

$$\sum_{i,j} \mathbf{D}_{i,j} \cdot (\mathbf{S}_i \times \mathbf{S}_j) \rightarrow \int \nabla \times (\mathbf{D} \cdot \mathbf{n}) \, dx dy$$

A vector calculus identity can be applied:

$$E_{DM} = \int (\nabla \cdot \mathbf{D}) \times \mathbf{n} - \mathbf{D} \cdot (\nabla \times \mathbf{n}) \, dx dy$$

In the desired case, $\mathbf{D} = -D \mathbf{n}$ and hence the final form for the second term is given by;

$$E_{DM} = \int D(\mathbf{n} \cdot \nabla \times \mathbf{n}) \, dx dy$$

Combing both terms leaves the required energy functional eq.(1.7).

5.1.2 A.2 One-constant approximation

The one elastic constant approximation for the Frank free energy is given by;

$$E = \frac{K}{2} \int_{\mathbb{R}} [(\nabla \cdot \mathbf{n})^2 + (q_0 + \mathbf{n} \cdot \nabla \times \mathbf{n})^2 + ((\mathbf{n} \cdot \nabla) \mathbf{n})^2] \, dx dy \quad (5.2)$$

Which may be expanded:

$$E = \frac{K}{2} \int_{\mathbb{R}} [(\nabla \cdot \mathbf{n})^2 + (\mathbf{n} \cdot \nabla \times \mathbf{n})^2 + 2q_0(\mathbf{n} \cdot \nabla \times \mathbf{n}) + q_0^2 + ((\mathbf{n} \cdot \nabla) \mathbf{n})^2] \, dx dy \quad (5.3)$$

The collection of terms

$$(\nabla \cdot \mathbf{n})^2 + (\mathbf{n} \cdot \nabla \times \mathbf{n})^2 + ((\mathbf{n} \cdot \nabla) \mathbf{n})^2$$

is equal to a customary definition of $|\nabla \mathbf{n}|^2$ [36];

$$|\nabla \mathbf{n}|^2 = (\nabla \cdot \mathbf{n})^2 + (\mathbf{n} \cdot \nabla \times \mathbf{n})^2 + ((\mathbf{n} \cdot \nabla) \mathbf{n})^2 - \nabla \cdot [\mathbf{n}(\nabla \cdot \mathbf{n}) - (\mathbf{n} \cdot \nabla) \mathbf{n}] \quad (5.4)$$

where the total divergence term is neglected¹². Hence;

$$E = \frac{K}{2} \int_{\mathbb{R}} |\nabla \mathbf{n}|^2 + 2q_0(\mathbf{n} \cdot \nabla \times \mathbf{n}) + q_0^2 dx dy \quad (5.5)$$

noting q_0^2 has no significance when E is minimised.

5.1.3 A.3 Derivative of Energy Functional

Starting at the simplified form of the free energy functional;

$$E = \int_D \left(\frac{K}{2} |\nabla \mathbf{n}|^2 + B(\mathbf{n} \cdot \nabla \times \mathbf{n}) \right) dA \quad (5.6)$$

to successfully locate the stationary points of functional given, Euler-Lagrange equations can be employed to find $\frac{\delta E}{\delta n}$ as a function of \mathbf{n} .

$$\frac{\delta E}{\delta n_i} = \frac{\partial L}{\partial n_i} - \nabla \cdot \frac{\partial L}{\partial \nabla n_i} \quad (5.7)$$

Where $i \in \{x, y, z\}$ and L is the function within the integral above. Here the case $i = y$ is used as an example, derivation of additional components follows exactly. Considering the first term of eq.(5.7):

$$\frac{\partial L}{\partial n_y} = \frac{K}{2} \frac{\partial}{\partial n_y} (|\nabla \mathbf{n}|^2) + B \frac{\partial}{\partial n_y} (\mathbf{n} \cdot \nabla \times \mathbf{n})$$

Note that $|\nabla \mathbf{n}|^2$ can be expressed as $\sum_i \partial_i \mathbf{n} \cdot \partial_i \mathbf{n}$ and therefore has no n_y dependence (only $\partial_i n_y$) leaving:

$$\frac{\partial L}{\partial n_y} = B \frac{\partial}{\partial n_y} (\mathbf{n} \cdot \nabla \times \mathbf{n})$$

$$= B(\partial_z n_x - \partial_x n_z)$$

Similarly the second term follows:

$$\frac{\partial L}{\partial \nabla n_y} = \frac{K}{2} \frac{\partial}{\partial \nabla n_y} (|\nabla \mathbf{n}|^2) + B \frac{\partial}{\partial \nabla n_y} (\mathbf{n} \cdot \nabla \times \mathbf{n})$$

With the first term easily evaluating to $K \nabla n_y$ and with some additional algebra the second term evaluates to $B(n_z \hat{\mathbf{i}} - n_z \hat{\mathbf{j}})$. Finally by taking the dot product with ∇ ,

$$\nabla \cdot \frac{\partial L}{\partial \nabla n_y} = K \nabla^2 n_y - B(\partial_z n_x - \partial_x n_z)$$

¹²Using Stoke's theorem a boundary integral is obtained and evaluated to 0.

and combining the first and second terms, we obtain a final solution for $\frac{\delta E}{\delta \mathbf{n}}$ in the y direction:

$$\frac{\delta E}{\delta n_y} = 2B(\partial_z n_x - \partial_x n_z) - K\nabla^2 n_y \quad (5.8)$$

Notice $(\partial_z n_x - \partial_x n_z)$ represents the y component of $\nabla \times \mathbf{n}$. This is in fact the case in all directions and hence we are able to write down the final form of $\frac{\delta E}{\delta \mathbf{n}}$:

$$\frac{\delta E}{\delta \mathbf{n}} = 2B(\nabla \times \mathbf{n}) - K\nabla^2 \mathbf{n} \quad (5.9)$$

5.1.4 A.4 Expected energy relationship

To approximate the relationship between minimum energy and B for an unconstrained system, it is reasonable to consider a system with zero splay ($\nabla \cdot \mathbf{n} = 0$), zero bend ($(\mathbf{n} \cdot \nabla)\mathbf{n} = 0$) and a twist with no preferred orientation. This simplifies the definition of $|\nabla \mathbf{n}|^2$ eq.(5.4) to:

$$|\nabla \mathbf{n}|^2 = (\mathbf{n} \cdot \nabla \times \mathbf{n})^2$$

Therefore the energy functional becomes:

$$E = \int \left[\frac{K}{2}(\mathbf{n} \cdot \nabla \times \mathbf{n})^2 + B(\mathbf{n} \cdot \nabla \times \mathbf{n}) \right] dA$$

In all cases considered within this project, $K_e = 1$ and so;

$$E = \int \frac{1}{2} \left[(\mathbf{n} \cdot \nabla \times \mathbf{n})^2 + 2B(\mathbf{n} \cdot \nabla \times \mathbf{n}) \right] dA$$

Then completing the square;

$$E = \int \frac{1}{2} \left[((\mathbf{n} \cdot \nabla \times \mathbf{n}) + B)^2 - B^2 \right] dA$$

The ground state eq.(1.12) satisfies $(\mathbf{n} \cdot \nabla \times \mathbf{n}) + B = 0$, therefore:

$$E_{\min} = \int -\frac{B^2}{2} dA$$

For the circular boundary conditions used eq.(2.6), this integral evaluates to:

$$E_{\min} = -\frac{\pi R^2 B^2}{2}$$

5.2 B: Tables

	$D(N)$	a	K	B	γ	Δt	σ
Effective	50	1	1	0.1 – 1.2	0.1	0.1	10^{-6}
Real	10 (μm)	N/A	3.25 (pN)	1.625 – 19.5 (μNm^{-1})	N/A	N/A	N/A

Table 2: Table of Simulation parameters relevant to the results and discussion (Section 3). Note, outside the diameter of the disk there's no contribution to the energy, therefore in our case, N and D are equivalent. For effective B values where $N \neq 50$ see table 3.

$B(\mu\text{Nm}^{-1})$	$B_e(N = 50)$	$B_e(N = 75)$	$B_e(N = 100)$	$p(\mu\text{m})$	D/p
1.625	0.1	0.067	0.05	12.56	0.80
3.25	0.2	0.133	0.1	6.28	1.59
4.875	0.3	0.2	0.15	4.19	2.36
6.5	0.4	0.267	0.2	3.14	3.18
8.125	0.5	0.333	0.25	2.51	3.98
9.75	0.6	0.4	0.3	2.09	4.77
11.375	0.7	0.467	0.35	1.79	5.57
13.0	0.8	0.533	0.4	1.57	6.37
14.625	0.9	0.6	0.45	1.39	7.16
16.25	1	0.667	0.5	1.25	7.96
17.875	1.1	0.733	0.55	1.14	8.75
19.5	1.2	0.8	0.6	1.05	9.55

Table 3: Table of effective B values used throughout the simulation process (Left) and the corresponding preferred length scale (helical pitch) p (Right).

$B(\mu\text{Nm}^{-1})$	$-CB^2$	$E_e(50)$	$E_e(75)$	$E_e(100)$	$E_e(150)$	$E_e(3\pi, 100)$	$E_e(5\pi, 100)$
1.625	-9.82	-6.07	-6.01	-5.90			
3.25	-39.27	-36.23	-35.81	-36.14		-79.93	-79.92
4.875	-88.36	-69.91	-69.76	-70.17		-154.33	-146.69
6.5	-157.08	-141.21	-139.68	-139.16		-237.61	-241.93
8.125	-245.44	-229.72	-226.42	-218.26	-236.88	-338.33	-348.82
9.75	-353.43	-326.43	-322.77	-338.27		-462.90	-476.40
11.375	-481.06	-454.86	-456.79	-462.89			
13	-628.32	-592.90	-591.33	-580.55			
14.625	-795.22	-745.26	-737.01	-774.53			
16.25	-981.75	-905.36	-918.20	-926.63			
17.875	-1187.91	-1083.00	-1115.07	-1124.06			
19.5	-1413.71	-1279.48	-1313.34	-1341.58			

Table 4: Table of effective energy values recorded throughout the analysis.

5.3 C: Supplementary Material

<https://github.com/DrDavie1/Skyrmions-under-Circular-Confinement>

All supplementary material is provided here within the zip file and link above. Videos mentioned within the report are given as mp4 files and must be downloaded to view:

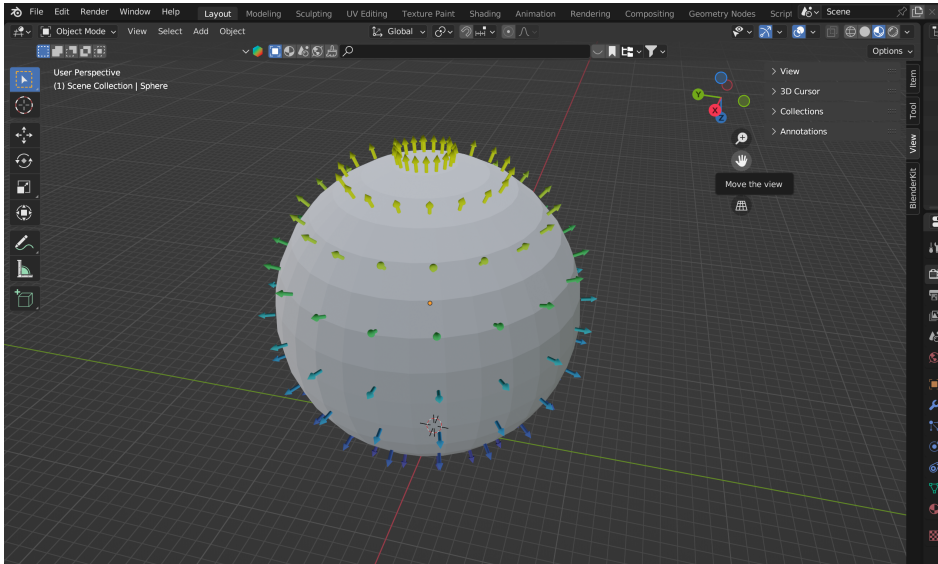
❖ Videos

- [Video A](#) : Sudden release of frustration via the Helfrich-Hurault (HH) instability ($N = 50, B_e = 0.4$)
- [Video B](#) : Initial observation of a Topological Change $Q = +1 \rightarrow Q = -3$. ($N = 50, B_e = 1.1$)
- [Video C](#) : Twist followed by undulations on the central skyrmion. ($N = 100, B = 9.75\mu\text{Nm}^{-1}$)
- [Video D](#) : Introduction of many twists with no evidence of undulations (not ran to stability) ($N = 150, B = 24.375\mu\text{Nm}^{-1}$)
- [Video E](#): Vanishing followed by stabilisation of twist (left) compared to vanishing twist observed by [Foster et al](#) (right).
- [Video F](#): Smooth removal of twist when the wavelength of initial twist is much smaller than helical pitch p .

Additional videos may be added to the 'additional content folder' after the reports submission.

The code provided includes the main minimisation algorithm and a file of initial state functions such as eq.(2.2, 2.2).

The creation of diagrams was completed using python, powerpoint and blender. Graphing code, particularly the creation of 3D vector fields is also provided.



Certification of ownership of the copyright

This Project Report is presented as part of, and in accordance with, the requirements for the degree of MSci/BSc (delete as applicable) at the University of Bristol, Faculty of Science.

I hereby assert that I own exclusive copyright in the item named below. I give permission to the University of Bristol Library to add this item to its stock and to make it available for consultation in the library, and for inter-library lending for use in another library. I also give consent for this report to made available electronically to staff and students within the University of Bristol. It may be copied in full or in part for any bona fide library or research work. No quotation and no information derived from it may be published without the author's prior consent.

Author	William Davie
Title	Structural Behavior of Two-Dimensional Skyrmions under Circular Confinement
Date of submission	18/05/2024

I agree that submission of this report constitutes signing of this declaration.

This project/dissertation is the property of the University of Bristol and may only be used with due regard to the rights of the author. Bibliographical references may be noted, but no part may be copied for use or quotation in any published work without the prior permission of the author. In addition, due acknowledgement for any use must be made.